Predicting the maximum spreading of a liquid drop impacting on a solid surface: Effect of surface tension and entrapped air layer

Thijs C. de Goede,[1,*] Karla G. de Bruin,[1,2] Noushine Shahidzadeh,[1] and Daniel Bonn[1,†]
[1]*Van der Waals–Zeeman Institute, Institute of Physics, University of Amsterdam, Science Park 904, 1098 XH Amsterdam, the Netherlands*
[2]*Netherlands Forensic Institute, Laan van Ypenburg 6, 2497 GB The Hague, the Netherlands*

(Received 14 August 2018; published 15 May 2019)

The spreading of liquid droplets impacting a surface at high speed is well understood by now. However, when a droplet impacts a surface at relatively low impact velocities (<1 m/s), the wetting properties of the fluid become important, and the entrapped air layer between the impacting drop and the solid surface prevents the immediate wetting of the surface. To determine the influence of both wetting and the entrapped air, we perform experiments by systematically varying the surface tension of the liquid and the air pressure. Drop impact measurements at reduced air pressures show that the spreading is independent of the pressure; dynamic contact-angle measurements indicate that this happens because the air film breaks rapidly. By varying the surface tension and surface wettability, we show that droplet spreading at low velocities can be predicted from the wetting properties of the surface and the known energy balance for the impact.

DOI: 10.1103/PhysRevFluids.4.053602

I. INTRODUCTION

Droplet impact has recently attracted much attention because of its key roles in processes of practical importance such as rain drops impacting on porous stone [1,2], spray cooling of hot surfaces [3,4], crop spraying [5,6], inkjet printing [7,8], and bloodstain pattern analysis in forensic research [9–11]. Although it is a commonly occurring phenomenon in our daily lives, the dynamics behind droplet spreading is still incompletely understood because of the intricate interplay among inertial, capillary, and viscous forces during impact, as well as the importance of the air viscosity for, e.g., droplet splashing [12].

In recent decades, there has been much discussion about how to relate the maximum spreading diameter $D_{\max}$ of an impacting drop to its impact velocity v_{imp}, its volume (given in terms of the droplet's initial diameter D_0), and the fluid parameters of the droplet. Most models can be divided into two regimes where either the viscous or capillary force dominates, commonly referred to as the viscous [13–18] and capillary [18–21] regimes, respectively. Recently, Eggers *et al.* stated that the droplet spreading cannot be fully described by either of the two regimes alone because most experiments probe a regime in which inertial, viscous, and capillary forces all contribute [22]. Laan *et al.* expanded on this work by quantifying the interpolation between two scaling models for the capillary regime ($\frac{D_{\max}}{D_0} \propto \text{We}^{\frac{1}{2}}$) [19] and the viscous regime ($\frac{D_{\max}}{D_0} \propto \text{Re}^{\frac{1}{5}}$) [13,16] using a first-order Padé approximant [23]. Here, We and Re are the Weber ($\text{We} \equiv \frac{\rho D_0 v_{\text{imp}}^2}{\sigma}$) and Reynolds ($\text{Re} \equiv \frac{\rho D_0 v_{\text{imp}}}{\mu}$) numbers, respectively, with ρ being the density, σ being the surface tension, and μ

*T.C.deGoede@uva.nl
†D.Bonn@uva.nl

being the viscosity of the fluid. By comparing a large number of experiments, these authors firmly established a predictive spreading model relating the spreading ratio ($\beta_{\max} \equiv \frac{D_{\max}}{D_0}$) of a droplet to its volume, impact velocity, and the fluid parameters.

In this study, we are concerned with the regime where the models discussed above break down, which is at low impact velocities: When the impact velocity, and thus both Re and We, go to zero, all the scaling models predict, by definition, a vanishing maximum spreading ratio. Evidently, this is unphysical since at zero impact velocity, a drop of a given volume should have a radius determined by the contact angle of the liquid on the substrate. Thus, the model of Laan *et al.* is limited to sufficiently high impact velocities, which fortunately corresponds to most drop impact experiments in practical situations. To also account for low-velocity impacts, Lee *et al.* modified the spreading model of Laan *et al.* by incorporating a nonzero value of the maximum spreading diameter at zero impact velocity (defined as β_0) into the dynamic droplet spreading model [24] and showed that this modification allows us to completely explain all drop impact experiments on different surfaces. This extra feature to the model of Laan *et al.* then uses the maximum radius after impact extrapolated to zero impact velocity in order to collapse all the data for different impact speeds, fluids, and surfaces onto a single curve. The extra parameter β_0 can be obtained directly from the impact experiments but is nonuniversal: It depends on the wetting properties of the surface, as wetting becomes prominent at low impact velocities. This then precludes an *a priori* prediction of the outcome of an impact experiment from the fluid properties and the kinetic energy of the drop.

Lee *et al.* showed that there indeed is a significant influence of the surface tension of the liquid but also that the results are rather insensitive to the nature of the solid surface. They proposed that this insensitivity was due to an entrapped air film preventing the droplet from making contact with the surface [25]. This hypothesis is plausible since recent work has shown that the atmospheric conditions have a significant influence on droplet dynamics, as, for example, in droplet splashing [12,26–30], air entrainment [31–33], the coalescence of droplets on liquid surfaces [34], air cushioning of an impacting drop [35,36,38], and bouncing droplets on superhydrophobic and hydrophilic surfaces [37,38]. In many cases, it was shown that an impacting drop does indeed skate over an entrapped air layer before wetting the surface [38–42]. Thus, the open questions are (i) whether the air film has a significant influence on low-velocity droplet impact and (ii) how the extra parameter introduced by Lee *et al.* can be related to the wetting properties of the fluid [43] so that the maximum radius can be predicted from the combined models of Laan *et al.* and Lee *et al.*

Here, we address these questions by comparing water drop impact experiments at different air pressures. With these experiments, we show that the entrapped air film does not have an influence on droplet spreading. By systematically varying the surface tension and changing the wettability of the substrate, we show that the advancing contact angle can be used to predict the maximum spreading extrapolated to at zero impact speed. The contact angle can be determined from the known wetting properties of the surface and the liquid surface tension, therefore allowing to fully predict the outcome of a low-velocity drop impact experiment.

II. MATERIALS AND METHODS

A. Surfaces and liquids

In order to systematically vary the liquid's surface tension at constant density and viscosity, nine different ethanol-water mixtures were used. The ethanol concentration (in weight percentage), density, surface tension, and viscosity of these mixtures are given in Table I.

To reveal the influence of surface wettability, we studied the impact of droplets onto three different surfaces: a microscope glass slide with a high wettability (Corning glass), stainless steel, and a candle-soot-based amphiphobic surface [44]. The stainless steel surface has an average surface roughness R_a of 0.247 ± 0.007 μm, as measured with a laser microscope (Keyence VK-X1000).

TABLE I. Fluid parameters values of water, ethanol, and ethanol-water mixtures, sorted by ethanol weight percentage (wt%). Sources: Refs. [45,46].

wt (%)	Density ($\frac{\text{kg}}{\text{m}^3}$)	Surface tension ($\frac{\text{mN}}{\text{m}}$)	Viscosity (mPas)
0	997.0	71.99	0.89
5	989.0	56.41	1.228
10	981.9	48.14	1.501
15	975.3	42.72	1.822
20	968.7	37.97	2.142
40	935.3	30.16	2.846
60	891.1	26.23	2.547
80	843.6	23.82	1.881
100	789.3	21.82	1.203

B. Sessile drop method

The wetting properties of a surface can be quantified by the equilibrium contact angle of a liquid drop deposited on the surface [43], which can be measured using the sessile drop method [47,48]. Because of surface inhomogeneities, the droplet has no unique contact angle but exhibits a range of contact angles on the surface. Therefore, we measured the maximum and minimum contact angles for which the droplet maintains a constant base diameter on the surface, also known as the advancing (θ_a) and receding (θ_r) contact angles, respectively. They were determined by adding or removing fluid to or from a deposited droplet until the droplet's base diameter changed. For each liquid, measurements were performed twice, and the errors in the measurements are given by the standard deviation. While this method was used for glass and stainless steel, for the amphiphobic surface, the contact angle reported by Deng *et al.* was used [44].

C. Drop impact

To investigate droplet impact, a syringe was suspended above a surface at height h. Blunt-tipped needles with a diameter of 0.4 mm were used to generate droplets with a D_0 between 1.7 and 2.2 mm depending on the surface tension of the fluid [49]. The impact and dynamics after impact were recorded with a high-speed camera (Phantom Miro M310) with frame rates between 4400 and 16 000 frames per second and spatial resolutions between 11 and 17.7 microns per pixel. The time frame used for measuring droplet impact was roughly between 10 and 30 ms starting at the moment of impact. Since the droplet is accelerated by gravity (g), the impact velocity (v_{imp}) can be controlled by changing the height (h): $v_{\text{imp}} \approx \sqrt{2gh}$. For each height, we repeated the measurements three times, averaging the outcomes (v_{imp}, D_0, and D_{max} as determined from the high-speed images), with the standard deviation as measurement error. To investigate the influence of air pressure, the droplet impact was measured inside a vacuum chamber at different pressures between 1000 mbar (atmospheric pressure) and 85 mbar. For low-velocity impacts, the dynamic contact angle during spreading was determined from each frame using the angle tool of the IMAGEJ software.

III. RESULTS AND DISCUSSION

To investigate the dynamics of low-velocity droplet impact, the dynamic contact angles on the left and right sides of the droplet (θ_L and θ_R, resp.) of water [Figs. 1(a1)–1(a4)] and ethanol [Figs. 1(b1)–1(b4)] on stainless steel were measured as a function of time with $t = 0$ being the moment the droplet reaches maximum spreading. In the early stages of the impact [Figs. 1(a2) and 1(b2)], the measured dynamic contact angles are high ($\approx 160^\circ$) for both fluids. As shown in Fig. 1(c), after roughly 2 ms, a sudden drop in the contact angle of both liquids occurs, with the contact angle of water remaining on the order of 115° up to the moment of maximum spreading (indicated by the red

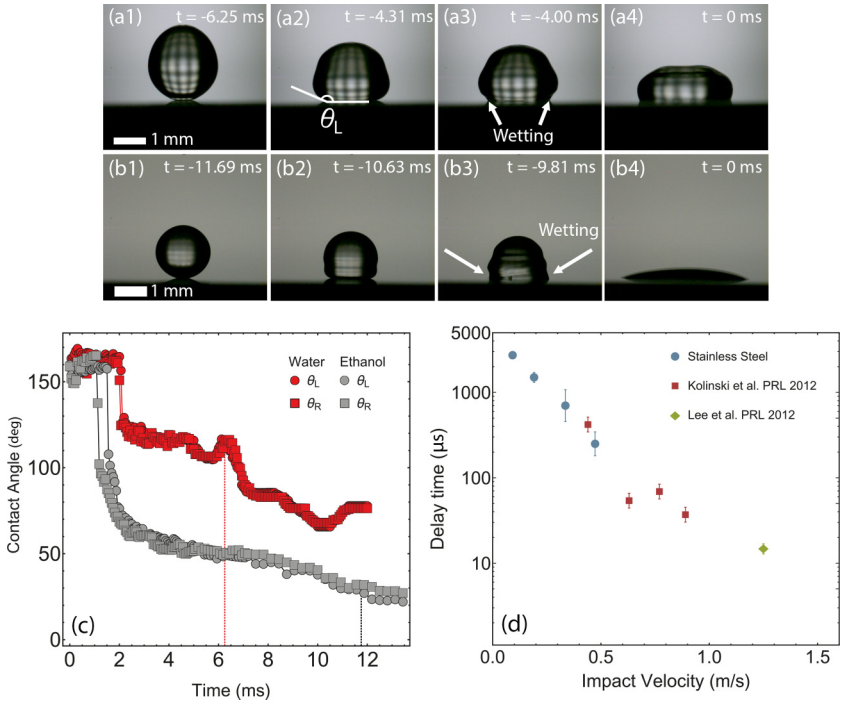

FIG. 1. Time evolution (left to right) of water [(a1)–(a4)] and ethanol [(b1)–(b4)] droplet impact at ≈ 0.1 m/s on stainless steel. During impact, the droplets do not immediately wet the surface but deform due to the presence of an air layer [(a2), (b2)]. A delayed wetting transition occurs due to the puncture of the entrapped air layer [(a3), (b3)], after which the droplet continues to spread until $D_{\max}$ is reached [(a4), (b4)]. $t = 0$ is the moment the droplet reaches maximum spreading. (c) Dynamic contact angle measurements of the water (red) and ethanol (gray) droplet from (a). The left and right contact angles θ_L and θ_R are given by the circles and squares, respectively. Dashed lines are inserted at the times of maximum spreading. (d) Measured time delay of the wetting transition (log-lin plot) of water on stainless steel (blue circles), compared to the air film lifetime measured by Kolinski *et al.* [41] and Lee *et al.* [50].

dashed line) and then decreasing to below 90°. In contrast, the dynamic contact angle for ethanol is much smaller and strongly decreases in time to a contact angle of the order of 30° at maximum spreading (black dashed line).

The high contact angles at the early stage of spreading suggests that droplets are spreading over the equivalent of a superhydrophobic surface ($\theta > 150°$) [51–53]. This "superhydrophobicity" of the surface is a result of a thin air film entrapped between the droplet and surface, as was first discussed by Mandre *et al.* [54] and Mani *et al.* [55]. Neglecting intermolecular forces between the droplet and surface, they hypothesized that during spreading the droplet compresses the gas underneath and creates a barrier between the droplet and surface. The presence of the air film has been experimentally demonstrated by several recent studies [40–42,56]. For our low-velocity impacts, we observe that the droplet does eventually penetrate the air film during spreading and comes into contact with the surface. A delayed wetting transition can be observed [Figs. 1(a3) and 1(b3)] that leads to the sharp decrease in the contact angle at around 2 ms [Fig. 1(c)]. This wetting transition delay is heavily dependent on the impact velocity of the droplet: Measuring the delay time of wetting for water as function of the impact velocity [blue circles in Fig. 1(d)] shows a significant decrease in the wetting delay for increasing impact velocity. Our measurements are limited to the velocity range of 0.1–0.5 m/s, as the delay time becomes shorter than the temporal resolution of the high-speed images. Interestingly, comparing our wetting time delay measurements

with the air film lifetime as measured by Kolinski *et al.* [41] (red squares) and Lee *et al.* [50] (green diamonds) suggests that the air film lifetime coincides with the wetting delay, with both following the same trend with increasing impact velocity. This indicates that the contact-angle decrease is indeed caused by the rupture of the air film.

In all our experiments, we observe that the air film ruptures. However, in other experiments, it has been reported that the air film can also remain intact during droplet impact. After reaching $D_{\max}$, the droplet then retracts and starts bouncing on the air film [37,38]. In this case, the droplet never makes contact with the surface, leading to a diverging delay time [38,57] instead of an finite delay for film rupture observed here. Whether the droplet punctures the air film or not during droplet impact is likely to depend on surface roughness and defects. It is likely that droplet spreading is different when the droplet spreads over a sustained air film or when the droplet punctures the air film, so it is important to note that this study only focuses on the air film influence on droplet spreading in the case of air film rupture during droplet impact.

We note that, during spreading on the air film, the droplet makes no contact with the surface, resulting in a contact angle of 180°, which is higher than is measured for the water and ethanol droplet before the wetting transition [Fig. 1(c)]. This is probably due to the spatial resolution of the image being too low to zoom in on the apparent contact region, resulting in a lower apparent contact angle.

In order to test whether the presence of the air film influences droplet spreading at low impact velocities, we studied water droplet impact at atmospheric (1000 mbar) and reduced (300 mbar) air pressures [Fig. 2(a)]. These experiments were done in a small vacuum chamber equipped with windows for light and camera access. At 300 mbar, the wetting transition (indicated by white arrows) occurs almost immediately after contact, in contrast to the delayed wetting transition observed at atmospheric pressure. This difference is evident from the dynamic contact angles measured at both pressures [Fig. 2(b)]: At reduced pressure, no sudden decrease in dynamic contact angle is observed. It is likely that the reduced pressure limits the ability of the air film to keep the droplet and surface separated and thus for wetting to occur almost immediately, i.e., faster than our experimental time resolution. Measurements of the maximum spreading ratio $\beta_{\max}$ for pressures down to 85 mbar [Fig. 2(c)] indicate that the spreading ratio does not change when the pressure is lowered. These results show that the delayed wetting and the initial presence of the air film does not have a significant influence on the maximum radius the droplet attains. The observation that low-velocity droplet spreading does not depend on air pressure appears to contrast with the recent study of splashing [12]. However, as the latter study was performed at higher impact velocities, it is likely that the influence of the surrounding air on droplet spreading is velocity dependent: The surrounding air only becomes influential at high velocities such as in case of air entrainment during coating [32,33] or when aerodynamic forces induce splashing [29,30,40].

Having established that for cases when the air film is punctured, low-velocity droplet spreading is independent of the surrounding air, the next question is whether β_0, the value of the maximum spreading diameter at zero impact velocity, can then be determined from the wetting properties of the surface. This can be evaluated by comparing the results of impact studies with what happens when a droplet is gently placed in contact ($v_{\text{imp}} \sim 0$) with the surface. In the latter case, the droplet starts to spread out and the resulting droplet configuration at mechanical equilibrium is governed by surface wettability and fluid surface tension. If we assume that the droplet attains a shape which is similar to a spherical cap [24,58], β_0 can be determined from the contact angle for both high and low wettability surfaces:

$$\beta_0 = \left[\frac{4\sin^3(\theta)}{2 - 3\cos(\theta) + \cos^3(\theta)}\right]^{1/3}, \qquad \theta < 90^\circ, \tag{1a}$$

$$\beta_0 = \left[\frac{1}{[2 + \cos(\theta)]\sin^4(\theta/2)}\right]^{1/3}, \qquad \theta > 90^\circ. \tag{1b}$$

A droplet gently deposited on a surface only stops spreading when its dynamic contact angle reaches a value equal to the advancing contact angle. Thus, we assume that at maximum spreading,

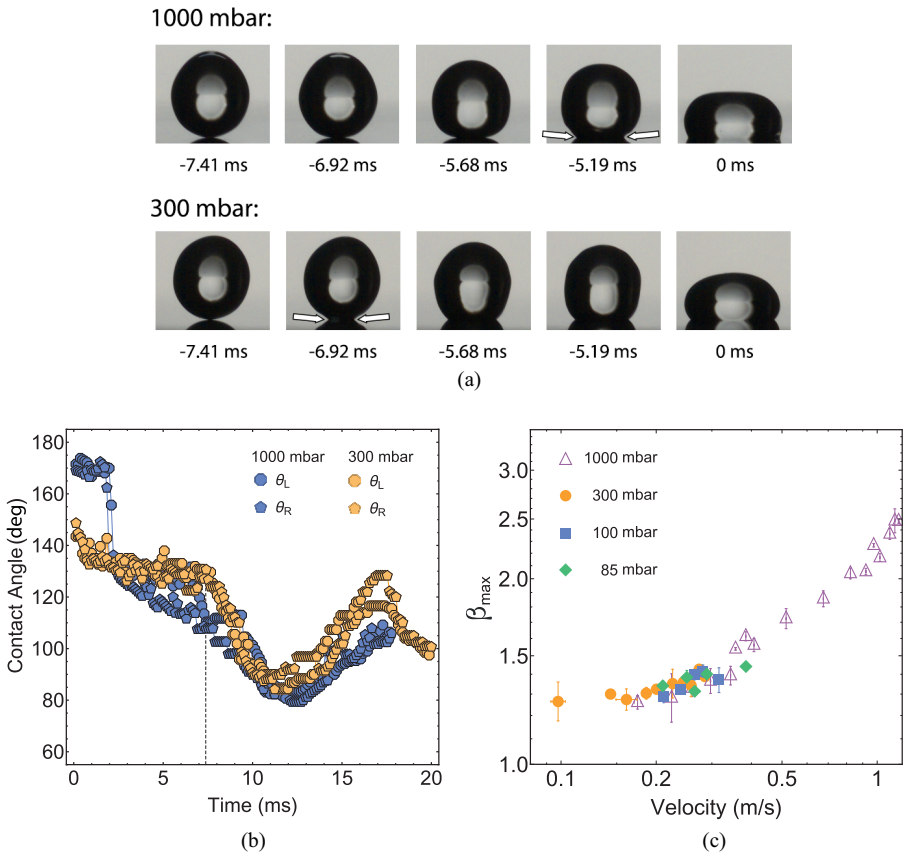

FIG. 2. (a) Water droplet impact on stainless steel at atmospheric (1000 mbar) and reduced (300 mbar) pressure for $v_{\text{imp}} \sim 0.1$ m/s. The white arrows indicate the wetting transition of the droplet. $t = 0$ is defined as the moment when the droplets reach maximum spreading. (b) Dynamic contact angle measurements of a water droplet impacting ($v_{\text{imp}} \sim 0.1$ m/s) stainless steel at atmospheric and reduced pressure. The dashed line shows the moment of the droplet reaching maximum spreading. (c) Spreading ratio of water on stainless steel at 1000 mbar (purple open upward triangles), 300 mbar (yellow circles), 100 mbar (blue squares), and 85 mbar (green diamonds) as function of impact velocity.

the contact angle of the spherical cap should be equal to the advancing contact angle of the liquid on the substrate. Therefore, only the advancing contact angle is considered for the calculation of β_0. To test the above hypothesis, we measured the contact angles and spreading ratios as a function of impact speed, extrapolated them to zero impact speeds of the evaluated fluids, and compared the values of β_0 obtained from both measurements.

The measured advancing and receding angles for each ethanol-water mixture on stainless steel are plotted as function of the surface tension in Fig. 3(a). All advancing contact angles are lower than 90°, indicating that the steel surface is partially wetting. The advancing contact angle of water on glass is $8° \pm 5°$. For the amphiphobic surface, we use the contact angle measured by Deng *et al.*, i.e., $165° \pm 5°$ [44].

The measured spreading ratios β_{max} of the different water-ethanol mixtures on stainless steel are plotted as a function of the impact velocity in Fig. 3(b). This graph clearly reveals a wetting effect at low impact speeds: The spreading ratio gradually decreases with increasing surface tension, from pure ethanol (blue circles) to water (purple upward triangles). At higher impact velocities, we approach the viscous-inertial regime for which the surface tension is unimportant. In this regime,

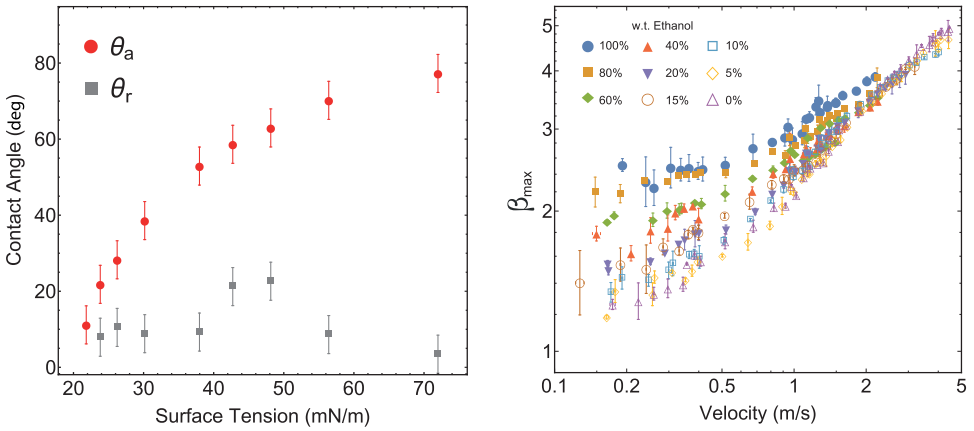

FIG. 3. (a) Advancing (θ_a; red circles) and receding (θ_r; gray squares) contact angles for each water-ethanol mixture on stainless steel plotted as a function of the liquid surface tension. (b) Maximum spreading ratio β_{max} as a function of impact velocity for each mixture impacting a stainless steel surface. In this figure, β_{max} was measured within a time frame of 30 ms after impact and long timescale wetting is not yet considered.

all liquids are expected to have a similar spreading due to the similarity in their viscosities, which is indeed observed in Fig. 3(b).

Changing the wettability of the surface also gives the same wetting effect at low impact speeds: When water impacts a high-wettability surface [top row of Fig. 4(a)], it behaves similarly to an ethanol droplet impacting a low-wettability surface [Fig. 1(b)]: The droplet impacts the air film and bulges outward until the air film is penetrated, after which the contact area between droplet and surface increases rapidly and extends until D_{max} is reached. For a non-wettable surface

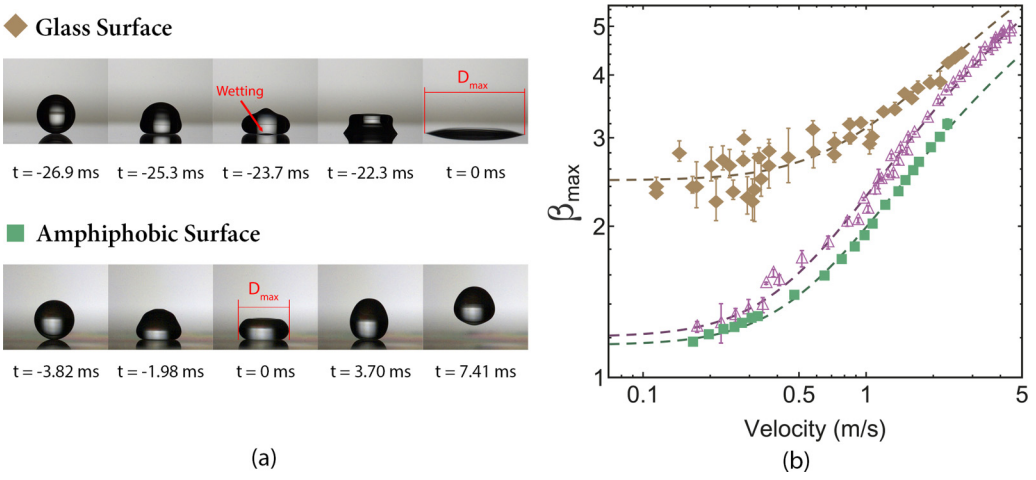

FIG. 4. (a) Water droplet impacting on hydrophilic glass (top) and an amphiphobic surface (bottom) at $v_{imp} \sim 0.22$ m/s. $t = 0$ is defined at the time when the spreading diameter is equal to D_{max}. (b) Spreading ratio as function of impact velocity of water droplets impacting on hydrophilic glass (brown diamonds) and the amphiphobic surface (green squares) compared to the stainless steel measurements (open upward purple triangles). The dashed lines are the best fits of Eq. (2). Again, β_{max} is determined within a timescale of 30 ms after impact, and the influence of long timescale wetting is currently neglected.

[bottom row of Fig. 4(a)], the liquid does not make contact with the surface and the droplet contracts after maximum spreading and bounces back up, similar to what has been observed for droplets bouncing on an air film [38]. Measuring the spreading ratio for these surfaces and comparing them to the spreading ratio of water on stainless steel [Fig. 4(b)] shows that increasing the wettability of the surface leads to the same wetting effect observed when the liquid surface tension is lowered. This effect, however, seems to be limited to contact angles lower than 90°, as the spreading ratio of the stainless steel and amphiphobic surface are similar.

Interestingly, the spreading curves of the glass and steel converge at higher impact velocities in contrast to those of stainless steel and the amphiphobic surface. Droplet spreading on the amphiphobic surface is less than the spreading ratio on stainless steel at higher impact velocities. This could be attributed to the extra viscous dissipation caused by the droplet bouncing on an air film [38]. As mentioned earlier, viscous dissipation is relatively unimportant at low impact velocities but becomes more significant at higher speeds. The extra viscous dissipation term therefore leads to a reduced spreading diameter of the droplet on the amphiphobic surface.

To determine β_0, which is the spreading ratio extrapolated to zero velocity, we turned to the spreading model proposed by Lee *et al.*, which gives the relation between the spreading ratio and the impact velocity as [24]

$$\sqrt{\beta_{\max}^2 - \beta_0^2}\,\mathrm{Re}^{-\frac{1}{5}} = \frac{\sqrt{\mathrm{We}}}{7.6 + \sqrt{\mathrm{We}}}. \tag{2}$$

Using the spreading model, the drop impact data shown in Figs. 3 and 4(b) were fitted by minimizing the square sum of residuals, using β_0 as a fitting parameter. To fit the spreading data of the amphiphobic surface, the extra viscous dissipation for droplet bouncing needs to be taken into account. Determining the amount of energy loss in droplet bouncing is an interesting topic on its own: de Ruiter *et al.* showed that a only a part of the extra energy dissipation is due to the viscous forces inside the air film [38]. The origin of the rest of this extra viscous dissipation is currently unknown and beyond the scope of this work. To account for the extra viscous dissipation, the viscosity of the fluid is used as a second fitting parameter, giving an "effective" viscosity. This effective viscosity contains all contributions to the viscous dissipation during impact. In Fig. 4(b), the best fits of (2) are given by the dashed lines, showing the droplet spreading data is fitted very well by the spreading model of Lee *et al.* In this study, the effective viscosity is assumed to be constant, but it is possible that the dynamics between the droplet and the air cushion could depend on the impact velocity, making the squeeze film dissipation in the air layer dependent on the Weber number. However, the good fit obtained from the spreading data on the amphiphobic surface [Fig. 4(b)] with a constant effective viscosity seems to suggest that any change in the squeeze film dissipation is negligible for droplet spreading in the measured range of impact velocities.

Figure 5(a) shows the best fit values of β_0 as function of the advancing contact angle for all ethanol-water mixtures on stainless steel (blue circles), water on the amphiphobic surface (green diamond), and water on glass (yellow square). Comparing the spherical cap model (red dashed line) to the drop impact measurements shows that the spherical cap model gives a reasonable prediction of β_0 for higher contact angles ($\theta_a > 20°$) but deviates from the droplet impact measurements at low contact angles.

To explain these deviations, we note that the spherical cap model assumes that the droplet attains a spreading ratio of β_0 when it is at mechanical equilibrium. For low contact angles, a droplet placed on the surface reaches mechanical equilibrium between seconds and several hours [43,49,59], taking significantly longer than the measured time frame of droplet impact as measured in Figs. 3(b) and 4(b). Measuring the spreading ratio for water and ethanol droplets on longer timescales [2000 fps; Fig. 5(b)] shows that for high-contact-angle cases (e.g., water), the droplets reach mechanical equilibrium quickly after impact but that for low-contact-angle cases (ethanol), the droplets do not reach mechanical equilibrium for at least several seconds. If the spreading ratio for low-velocity droplet spreading ($v_{\mathrm{imp}} < 1$ m/s) on hydrophilic glass is measured again but $D_{\max}$

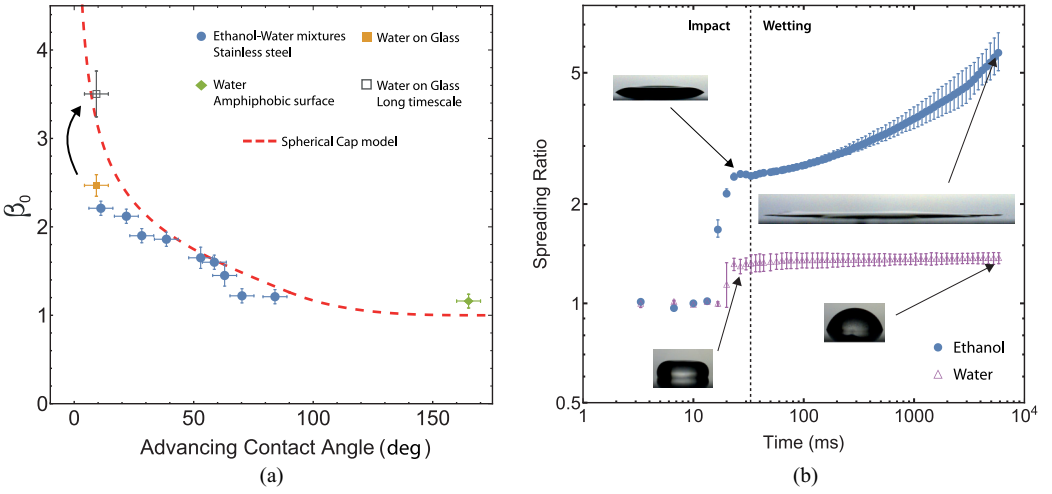

FIG. 5. (a) Spreading ratio at zero velocity as calculated from the spherical cap model (dashed red line) and β_0 values extrapolated from measurements on ethanol-water mixtures on steel (blue circles), water on glass (yellow filled square), and water on the amphiphobic surface (green diamond). Taking long timescale wetting into account, the β_0 value of water on glass (gray open square) is comparable to the prediction of the spherical cap model. (b) Long timescale spreading of water (purple triangles) and ethanol (blue circles) droplets on stainless steel. While water reaches its maximum spreading ratio quickly, the spreading of an ethanol droplet takes significantly more time. The inset images show the droplet shapes on the surface for short and long timescales.

is determined when the droplet reaches mechanical equilibrium, the newly extrapolated β_0 value [open gray square in Fig. 5(a)] is significantly higher and agrees well with the spherical cap model. This shows that surface wettability has a direct influence not only on the spreading diameter during impact [Figs. 4(b) and 5(b)] but also on the maximum spreading of a droplet at longer timescales and has to be taken into account for low-contact-angle droplet spreading at low impact velocity in order to use the spreading model of Lee *et al.* with the addition of the spherical cap model.

The spherical cap model also slightly underestimates the spreading ratio at zero velocity on the amphiphobic surface, which could be due to the droplet not obtaining a perfect pearl-like shape [60,61] on the surface. The characteristic length scale of the water droplet D_0 ($D_0 \approx 2.2$ mm) is comparable to the capillary length ($\sqrt{\sigma/\rho g} = 2.4$ mm, with g being the gravitational constant) of water. It is therefore likely that gravity influences the droplet shape somewhat by slightly flattening the droplet and thus increasing β_0 for water droplets on the amphiphobic surface. However, as our measurements do not cover droplet impact below 0.1 m/s, confirming whether gravity influences the droplet's shape at zero impact velocity is not possible in this study. However, the deviation between the spherical cap model and the measured β_0 of amphiphobic surface is relatively small such that the spherical cap model could still be used to give a reasonable prediction of β_0 for hydrophobic surfaces.

The results of this study are in stark contrast with the findings of Lee *et al.* They found no influence of surface wettability on droplet spreading [24] and attributed this to the entrapped air layer between the droplet and surface at low impact speeds [25]. Although this entrapped air layer exists in the early stages of impact, we showed it has no significant influence on droplet spreading and that surface wettability does influence droplet spreading. The reason for this discrepancy could be that Lee *et al.* characterized the surface wettability using the equilibrium contact angle. However, due to contact angle hysteresis, a range of angles between the receding and advancing contact angles can be measured for nonideal surfaces. It is possible that the advancing contact angles of the surfaces used by Lee *et al.* are similar to each other and therefore have a similar β_0 value as well. As Lee

et al. did not measure the receding and advancing contact angles, however, no definite conclusion can be given.

IV. CONCLUSIONS

We studied the influence of the entrapped air layer on droplet spreading by investigating droplet spreading at different air pressures. These measurements reveal that the entrapped air layer does not have a significant influence on the maximum spreading radius for the air pressures investigated (85–1000 mbar). Comparing contact angle and drop impact measurements, we show that droplet spreading at low impact velocity can be predicted from the wetting properties of the surface and liquid surface tension by assuming that the droplet attains a spherical cap shape at mechanical equilibrium. For low-contact-angle cases, we show that the slow wetting dynamics needs to be taken into account in order to accurately predict droplet spreading.

The observation that low-velocity droplet impact is independent of the air pressure suggests that the surrounding air only becomes important if the impact velocity is sufficiently high or if the air layer is not penetrated by the droplet. Furthermore, being able to predict droplet spreading at low velocities with the wetting properties of the surface and surface tension of the liquid allows for an easier and more accurate prediction of the spreading diameter of a droplet for any surface at low impact velocities, allowing for the inclusion of bloodstains formed at low impact velocity in the reconstruction of events at a crime scene [11].

ACKNOWLEDGMENT

We would like to thank J. Eggers and J. Sprittles for useful discussions regarding dynamic wetting at low velocities.

[1] N. Shahidzadeh-Bonn, S. Rafaı, D. Bonn, and G. Wegdam, Salt crystallization during evaporation: Impact of interfacial properties, Langmuir **24**, 8599 (2008).

[2] J. Lee, D. Derome, and J. Carmeliet, Drop impact on natural porous stones, J. Colloid Interface Sci. **469**, 147 (2016).

[3] R. P. Selvam, L. Lin, and R. Ponnappan, Direct simulation of spray cooling: Effect of vapor bubble growth and liquid droplet impact on heat transfer, Int. J. Heat Mass Transf. **49**, 4265 (2006).

[4] J. Kim, Spray cooling heat transfer: The state of the art, Int. J. Heat Fluid Flow **28**, 753 (2007).

[5] W. Wirth, S. Storp, and W. Jacobsen, Mechanisms controlling leaf retention of agricultural spray solutions, Pestic. Sci. **33**, 411 (1991).

[6] V. Bergeron, D. Bonn, J. Y. Martin, and L. Vovelle, Controlling droplet deposition with polymer additives, Nature (London) **405**, 772 (2000).

[7] Y. Son, C. Kim, D. H. Yang, and D. J. Ahn, Spreading of an inkjet droplet on a solid surface with a controlled contact angle at low Weber and Reynolds numbers, Langmuir **24**, 2900 (2008).

[8] B. Derby, Inkjet printing of functional and structural materials: Fluid property requirements, feature stability, and resolution, Annu. Rev. Mater. Res. **40**, 395 (2010).

[9] C. Knock and M. Davison, Predicting the position of the source of blood stains for angled impacts, J. Forensic, Sci. **52**, 1044 (2007).

[10] C. D. Adam, Experimental and theoretical studies of the spreading of bloodstains on painted surfaces, Forensic Sci. Int. **229**, 66 (2013).

[11] N. Laan, K. G. de Bruin, D. Slenter, J. Wilhelm, M. Jermy, and D. Bonn, Bloodstain pattern analysis: Implementation of a fluid dynamic model for position determination of victims, Sci. Rep. **5**, 11461 (2015).

[12] L. Xu, W. W. Zhang, and S. R. Nagel, Drop splashing on a dry smooth surface, Phys. Rev. Lett. **94**, 184505 (2005).

[13] J. Madejski, Solidification of droplets on a cold surface, Int. J. Heat, Mass Transfer **19**, 1009 (1976).
[14] S. Chandra and C. T. Avedisian, On the collision of a droplet with a solid surface, Proc. R. Soc. London, Ser. A **432**, 13 (1991).
[15] M. Pasandideh-Fard, Y. Qiao, S. Chandra, and J. Mostaghimi, Capillary effects during droplet impact on a solid surface, Phys. Fluids **8**, 650 (1996).
[16] I. V. Roisman, R. Rioboo, and C. Tropea, Normal impact of a liquid drop on a dry surface: Model for spreading and receding, Proc. R. Soc. London, Ser. A **458**, 1411 (2002).
[17] C. W. Visser, Y. Tagawa, C. Sun, and D. Lohse, Microdroplet impact at very high velocity, Soft Matter **8**, 10732 (2012).
[18] C. Clanet, C. Béguin, D. Richard, and D. Quéré, Maximal deformation of an impacting drop, J. Fluid. Mech. **517**, 199 (2004).
[19] E. W. Collings, A. J. Markworth, and J. K. McCoy, J. H. Saunders, Splat-quench solidification of freely falling liquid-metal drops by impact on a planar substrate, J. Mater. Sci. **25**, 3677 (1990).
[20] T. Bennett and D. Poulikakos, Splat-quench solidification: Estimating the maximum spreading of a droplet impacting a solid surface, J. Matter. Sci. **28**, 963 (1993).
[21] M. Aytouna, D. Bartolo, G. Wegdam, D. Bonn, and S. Rafaï, Impact dynamics of surfactant laden drops: Dynamic surface tension effects, Exp. Fluids **48**, 49 (2010).
[22] J. Eggers, M. A. Fontelos, C. Josserand, and S. Zaleski, Drop dynamics after impact on a solid wall: Theory and simulations, Phys. Fluids **22**, 062101 (2010).
[23] N. Laan, K. G. de Bruin, D. Bartolo, C. Josserand, and D. Bonn, Maximum diameter of impacting liquid droplets, Phys. Rev. Appl. **2**, 044018 (2014).
[24] J. B. Lee, N. Laan, K. G. de Bruin, G. Skantzaris, N. Shahidzadeh, D. Derome, J. Carmeliet, and D. Bonn, Universal rescaling of drop impact on smooth and rough surfaces, J. Fluid Mech. **786**, R4 (2015).
[25] J. Lee, Droplet Dynamics on non-porous and porous media, Ph.D. thesis, ETH Zurich, Zurich, Switzerland, 2015, https://www.research-collection.ethz.ch/handle/20.500.11850/155441.
[26] A. Latka, A. Strandburg-Peshkin, M. M. Driscoll, C. S. Stevens, and S. R. Nagel, Creation of Prompt and Thin-Sheet Splashing By Varying Surface Roughness or Increasing Air Pressure, Phys. Rev. Lett. **109**, 054501 (2012).
[27] C. S. Stevens, Scaling of the splash threshold for low-viscosity fluids, Europhys. Lett. **106**, 24001 (2014).
[28] C. S. Stevens, A. Latka, and S. R. Nagel, Comparison of splashing in high- and low-viscosity liquids, Phys. Rev. E **89**, 063006 (2014).
[29] G. Riboux and J. M. Gordillo, Experiments of Drops Impacting a Smooth Solid Surface: A Model of the Critical Impact Speed for Drop Splashing, Phys. Rev. Lett. **113**, 024507 (2014).
[30] T. C. de Goede, N. Laan, K. G. de Bruin, and D. Bonn, Effect of wetting on drop splashing of Newtonian fluids and blood, Langmuir **34**, 5163 (2017).
[31] A. Marchand, T. S. Chan, J. H. Snoeijer, and B. Andreotti, Air Entrainment by Contact Lines of a Solid Plate Plunged Into a Viscous Fluid, Phys. Rev. Lett. **108**, 204501 (2012).
[32] J. E. Sprittles, Air entrainment in dynamic wetting: Knudsen effects and the influence of ambient air pressure, J. Fluid Mech. **769**, 444 (2015).
[33] J. E. Sprittles, Kinetic Effects in Dynamic Wetting, Phys. Rev. Lett. **118**, 114502 (2017).
[34] N. Vandewalle, D. Terwagne, K. Mulleners, T. Gilet, and S. Dorbolo, Dancing droplets onto liquid surfaces, Phys. Fluids **18**, 091106 (2006).
[35] R. C. van der Veen, T. Tran, D. Lohse, and C. Sun, Direct measurements of air layer profiles under impacting droplets using high-speed color interferometry, Phys. Rev. E **85**, 026315 (2012).
[36] J. de Ruiter, J. M. Oh, D. van den Ende, and F. Mugele, Dynamics of Collapse of Air Films in Drop Impact, Phys. Rev. Lett. **108**, 074505 (2012).
[37] J. M. Kolinski, L. Mahadevan, and S. M. Rubinstein, Lift-Off Instability During the Impact of a Drop on a Solid Surface, Phys. Rev. Lett. **112**, 134501 (2014).
[38] J. de Ruiter, R. Lagraauw, D. van den Ende, and F. Mugele, Wettability-independent bouncing on flat surfaces mediated by thin air films, Nat. Phys. **11**, 48 (2015).

[39] P. Dell'Aversana, V. Tontodonato, and L. Carotenuto, Suppression of coalescence and of wetting: The shape of the interstitial film, Phys. Fluids **9**, 2475 (1997).
[40] M. M. Driscoll and S. R. Nagel, Ultrafast Interference Imaging of Air in Splashing Dynamics, Phys. Rev. Lett. **107**, 154502 (2011).
[41] J. M. Kolinski, S. M. Rubinstein, S. Mandre, M. P. Brenner, D. A. Weitz, and L. Mahadevan, Skating on a Film of Air: Drops Impacting on a Surface, Phys. Rev. Lett. **108**, 074503 (2012).
[42] H. Y. Lo, Y. Liu, and L. Xu, Mechanism of Contact Between a Droplet and an Atomically Smooth Substrate, Phys. Rev. X **7**, 021036 (2017).
[43] D. Bonn, J. Eggers, J. Indekeu, J. Meunier, and E. Rolley, Wetting and spreading, Rev. Mod. Phys. **81**, 739 (2009).
[44] X. Deng, L. Mammen, H.-J. Butt, and D. Vollmer, Candle soot as a template for a transparent robust superamphiphobic coating, Science **335**, 67 (2012).
[45] W. M. Haynes, *CRC Handbook of Chemistry and Physics* (CRC Press, Boca Raton, FL, 2014).
[46] G. Vazquez, E. Alvarez, and J. M. Navaza, Surface tension of alcohol + water from 20 to 50 degree C, J. Chem. Eng. Data **40**, 611 (1995).
[47] J. Bachmann, A. Ellies, and K. Hartge, Development and application of a new sessile drop contact angle method to assess soil water repellency, J. Hydrol. **231-232**, 66 (2000).
[48] J. Bachmann, R. Horton, R. Van Der Ploeg, and S. Woche, Modified sessile drop method for assessing initial soil–water contact angle of sandy soil, Soil Sci. Soc. Am. J. **64**, 564 (2000).
[49] P. De Gennes, F. Brochard-Wyart, and D. Quéré, *Capillarity and Wetting Phenomena: Drops, Bubbles, Pearls, Waves* (Springer Science & Business Media, Berlin, 2004).
[50] J. San Lee, B. M. Weon, J. H. Je, and K. Fezzaa, How does an Air Film Evolve Into a Bubble During Drop Impact? Phys. Rev. Lett. **109**, 204501 (2012).
[51] X.-M. Li, D. Reinhoudt, and M. Crego-Calama, What do we need for a superhydrophobic surface? A review on the recent progress in the preparation of superhydrophobic surfaces, Chem. Soc. Rev. **36**, 1350 (2007).
[52] R. S. Voronov, D. V. Papavassiliou, and L. L. Lee, Review of fluid slip over superhydrophobic surfaces and its dependence on the contact angle, Ind. Eng. Chem. Res. **47**, 2455 (2008).
[53] Y. Y. Yan, N. Gao, and W. Barthlott, Mimicking natural superhydrophobic surfaces and grasping the wetting process: A review on recent progress in preparing superhydrophobic surfaces, Adv. Colloid Interface Sci. **169**, 80 (2011).
[54] S. Mandre, M. Mani, and M. P. Brenner, Precursors to Splashing of Liquid Droplets on a Solid Surface, Phys. Rev. Lett. **102**, 134502 (2009).
[55] M. Mani, S. Mandre, and M. P. Brenner, Events before droplet splashing on a solid surface, J. Fluid Mech. **647**, 163 (2010).
[56] J. de Ruiter, D. van den Ende, and F. Mugele, Air cushioning in droplet impact. II. Experimental characterization of the air film evolution, Phys. Fluids **27**, 012105 (2015).
[57] J. M. Kolinski, L. Mahadevan, and S. Rubinstein, Drops can bounce from perfectly hydrophilic surfaces, Europhys. Lett. **108**, 24001 (2014).
[58] E. Berthier and D. J. Beebe, Flow rate analysis of a surface tension driven passive micropump, Lab Chip **7**, 1475 (2007).
[59] L. Tanner, The spreading of silicone oil drops on horizontal surfaces, J. Phys. D **12**, 1473 (1979).
[60] J. Bico, C. Marzolin, and D. Quéré, Pearl drops, Europhys. Lett. **47**, 220 (1999).
[61] D. Richard and D. Quéré, Bouncing water drops, Europhys. Lett. **50**, 769 (2000).